Final Draft
of the original manuscript:

Du, F.; Hoenzke, S.; Neumann, F.; Keilitz, J.; Chen, W.; Ma, N.; Hedtrich, S.; Haag, R.:

Development of biodegradable hyperbranched core-multishell nanocarriers for efficient topical drug delivery

In: Journal of Controlled Release (2016) Elsevier

DOI: 10.1016/j.jconrel.2016.06.048

Development of Biodegradable Hyperbranched Core-Multishell Nanocarriers for Efficient Topical Drug Delivery

*Fang Du,[a] Stefan Hönzke,[b] Falko Neumann,[a,c] Juliane Keilitz,[a] Wei Chen,[a] Nan Ma,[a,c] Sarah Hedtrich,[b] Rainer Haag [a]**

[a]*Institut für Organische Chemie und Biochemie, Freie Universität Berlin, Takustraße 3, 14195 Berlin, Germany*

[b]*Institute of Pharmacy (Pharmacology and Toxicology), Freie Universität Berlin, 14195 Berlin, Germany*

[c]*Institute of Biomaterial Science, Helmholtz-Zentrum Geesthacht, 14513 Teltow, Germany*

**Corresponding author*

E-mail address: haag@chemie.fu-berlin.de

The topical application of drugs allows for a local application in skin disease and can reduce side effects. Here we present biodegradable core-multishell (CMS) nanocarriers which are composed of a hyperbranched polyglycerol core functionalized with diblock copolymers consisting of polycarprolacton (PCL) and poly(ethylene glycol) (mPEG) as the outer shell. The anti-inflammatory drug dexamethasone (Dexa) was loaded into these CMS nanocarriers. DLS results suggested that Dexa loaded nanoparticles mostly act as a unimolecular carrier system. With longer PCL segments,

a better transport capacity is observed. *In vitro* skin permeation studies showed that CMS nanocarriers could improve the Nile red penetration through the skin by up to 7 times, compared to a conventional cream formulation. Interestingly, covalently FITC-labeled CMS nanocarriers remain in the stratum corneum layer. This suggests the enhancement is due to the release of cargo after being transported into the stratum corneum by the CMS nanocarriers. In addition, the hPG-PCL-mPEG CMS nanocarriers exhibited good stability, low cytotoxicity, and their production can easily be scaled up, which makes them promising nanocarriers for topical drug delivery.

Keywords: Topical application, dexamethasone, core-multishell (CMS) nanocarriers, drug delivery systems

1. Introduction

Over the past few decades, topical drug delivery has attracted much interest and has been considered as a potential alternative to traditional oral and intravenous drug delivery systems especially for skin diseases [1]. It offers numerous advantages, including noninvasive treatment, easy application, improved patient compliance, decreased systemic side effects, and improved drug bioavailability due to an avoidance of the degradation from a hepatic first-pass metabolism or digestion system [2]. However, a major concern is the low permeability of drugs through skin layers due to the excellent protective function of the highly packed lipid structure in the stratum corneum (SC), the outermost layer of skin. Previous reports showed only a limited

number of drugs with optimal physicochemical properties, for example, low molecular weight (< 500 Da) and proper lipophilicity, could be passively transported through the SC, which significantly hinders the successful topical treatment of some skin diseases [3].

Up to now, many skin penetration enhancement strategies have been developed to improve the topical delivery of drugs either with physical techniques, such as microneedles [4], iontophoresis [5], and sonophoresis [6], or by using chemical methods such as co-solvent systems [7] and nanoscale carriers [8, 9]. Among these strategies, polymeric nanocarriers have been focused on as a kind of chemical penetration enhancers. They are convenient for self-administration and suitable for applications to a large area of the body. Compared to other colloidal delivery systems such as liposomes [8] and lipid nanoparticles [9], polymeric core-shell nanocarriers display improved stability and avoid using small molecular weight surfactants which can penetrate deep into skin and cause irritation or systemic absorption [10]. At the same time, they can also protect labile pharmaceutical agents from premature degradation [11]. Furthermore, drug loading capacity and controlled release can be easily achieved by modifying the polymer composition. For topical delivery, pharmaceutical agents are incorporated into the polymeric carriers, where aggregates of 100 − 200 nm in diameter usually form. Although this size range allows some accumulation of particles in the appendages, e.g., hair follicles, most of the particles are eliminated by daily washing due to the low penetration ability. On the basis of previous knowledge that the vertical and lateral gaps between corneocytes present in the stratum

corneum are about 19 nm [12], small sized particles (< 30 nm) have been found to penetrate easier and faster than bigger ones (> 100 nm) due to the higher surface-to-volume ratio that can facilitate the interaction with the skin layer [13]. A few examples of drug carriers of 20 − 40 nm in size have been reported, which all utilize polymer micelles generated by self-assembly [14, 15]. Thermodynamic stability of these micelles during formulation and administration is still an issue. Therefore, a biodegradable polymeric nanocarrier system that has an ultrasmall size (< 30 nm) and is highly thermodynamic stable for topical drug delivery would be desirable.

Dendritic core-multishell (CMS) nanocarriers that are based on a dendritic polymer core covalently linked to amphiphilic, linear double shells exhibit excellent stability. By tuning the balance of the hydrophilic and hydrophobic parts, small unimolecular nanocarriers with the size range of 8 − 20 nm could be achieved. In our previous work, a liposome-inspired CMS nanocarrier consisting of a polar hyperbranched polyglycerol core surrounded by a C18-alkyl chain inner shell and monomethoxypoly(ethylene glycol) outer shell was fabricated [16, 17]. This kind of nanocarrier enabled the transport of hydrophobic (Nile red, pyrene, Dox) and hydrophilic guest molecules (Congo red, Rhodamine B) in both polar and nonpolar solvents and exhibited both good tumor targeting and skin penetration enhancement abilities [18-20]. Concerning the long-term safety and to improve the drug loading capacity, we now designed and synthesized a series of biodegradable CMS nanocarriers (Fig. 1). The highly bioinert hyperbranched polyglycerol (hPG) was introduced as a core. It not only provides multiple functional groups, but can also interact with the

"polar heads" of skin lipids to increase the size of "water pores", since many polar groups (alcohol, amine) are presented on the surface of hPG. The biodegradable poly(ε-caprolactone) (PCL) as the inner shell was incorporated to achieve tunable particle size and drug loading capacity as well as to improve the skin permeability by interacting with the "nonpolar tails" of the skin lipids. The outer shell is monomethoxypoly(ethylene glycol) (mPEG), which can stabilize the nanocarriers in water and prevents the formation of large aggregates. Properties regarding their aggregation behaviors and encapsulation capacities of the anti-inflammatory drug Dexamethason (Dexa) were systematically investigated and compared with their linear mPEG-PCL counterparts. In vitro studies, including cytotoxicity and skin penetration ability, were conducted to extensively evaluate the potential of the unimolecular CMS as promising drug nanocarriers for topical drug delivery.

2. Materials and methods

2.1. Materials

hPG amine (Mn 10,000 g/mol) was prepared with 70% amination according to the published method [21]. ε-Caprolactone (97%; Sigma-Aldrich) was dried over calcium hydride (CaH_2) and distilled under reduced pressure before use. Stannous 2-ethylhexanoate ($Sn(Oct)_2$), succinic anhydride, 4-dimethylamino pyridine (DMAP), diisopropylethylamin (DIPEA), Poly(ethylene glycol) methyl ether (mPEG, M_n ~2000 g mol^{-1}), *O*-(*N*-Succinimidyl)-*N*,*N*,*N*′,*N*′ tetramethyluronium-hexafluorophosphate

(HSTU), dimethylformamide (DMF), and dimethylsulfoxid (DMSO) were purchased from Sigma-Aldrich.

2.2 Characterizations

NMR spectra were recorded on a Bruker ECX 400 (^{1}H: 400 MHz, ^{13}C: 100 MHz). The molecular weight was measured by gel permeation chromatography (GPC), using DMF with 0.3% LiBr and 0.6% acetic acid as the mobile phase at a flow rate of 1 mL min^{-1}. The size of the carriers was determined by dynamic light scattering (DLS) at 25 °C using a Zetasizer Nano-ZS 15 from Malvern Instruments equipped with a 633 nm He–Ne laser. The melting points of the polymers were determined using a Linseis STA PT1600 differential scanning calorimeter (DSC). The samples were heated at a rate of 10 °C /min. Cryogenic transmission electron microscopy (Cryo-TEM) samples were prepared on copper grids (400 mesh) covered by a collodion film and vapor deposition of 7 nm carbon and visualized using a FEI CM12 electron microscope. The HPLC measurements of Dexamethasone were carried out on a Knauer Smartline-HPLC system, equipped with a RP-18 column (250 mm x 4 mm, 5 µm particle size) and UV-Vis detector (λ= 245 nm). The mobile phase is an acetonitril-water (40:60, v/v) mixture and the flow-rate is 1 mL min^{-1}.

2.2. Synthesis of monohydroxy-terminated diblock copolymers mPEG-PCL$_m$-OH

Monohydroxy-terminated diblock copolymers were synthesized by ring-opening polymerization of ε-caprolactone using mPEG as a macroinitiator and Sn(Oct)$_2$ as a

catalyst. Briefly, 1 g of mPEG (0.5 mmol, M_n = 2000 g/mol) was placed in a Schlenk flask and dried under high vacuum at 70 °C overnight. At room temperature, 0.27 − 1.1 ml of distilled ε-caprolactone (5, 10, 20 eq) and a catalytic amount of $Sn(Oct)_2$ were added under argon atmosphere. After exchanging the vacuum and argon three times, the system was heated to 120 °C and stirred for 24 h under argon atmosphere. The polymerization was quenched by cooling to room temperature. 10 ml of DCM were added to dissolve the polymer, together with one drop of acetic acid. The resulting solution was precipitated into a large amount of cold diethyl ether. The final product was collected by filtration and dried under high vacuum overnight (Yield: 90 - 95%).

2.3. Synthesis of carboxyl group-terminated diblock copolymers mPEG-PCL_m-COOH

Taking Shell 2 as an example, the other two shells were synthesized by the same method. Briefly, 1 g of mPEG-PCL_{10}-OH (0.3 mmol) and 67 mg of DMAP (0.6 mmol) were dissolved in anhydrous THF (20 mL). Then 300 mg of succinic anhydride (3 mmol) was added and the reaction stirred at room temperature for 48 h. Thereafter, the mixture was kept at −20 °C for several hours and filtered to remove the excess succinic anhydride. The filtrate was then precipitated into cold methanol/diethyl ether (1:1, v/v) mixture for three times (Yield: 70 - 85%).

2.4. Synthesis of hyperbranched core-multishell copolymers HPG-PCL_m-mPEG

The final CMS copolymers were synthesized by amide coupling chemistry. Taking CMS 2 (hPG-PCL_{10}-mPEG) as an example, 1 g of mPEG-PCL_{10}-COOH (0.3 mmol)

was dissolved in 5 ml of anhydrous DMF, which was followed by adding 30 µl of DIPEA (1.2 mmol) and 144 mg of HSTU (0.4 mmol). The mixture was protected by argon atmosphere and stirred at room temperature for 48 h to activate the acid. 21 mg of hyperbranched polyglycerol amine (hPG-NH_2, 0.2 mmol, M_n = 10 kDa) in 1 ml of DMSO was added to the resulting solution. The reaction was carried out for another 48 h. The crude CMS was purified first by dialysis against the mixed solvent of methanol and chloroform (1:1, v/v) using the dialysis bag (MWCO 4 - 6 kDa) to remove DMF and the coupling agents. After changing the dialysis media 3 times, the solution in dialysis bag was collected and concentrated. In order to get rid of the free double shells, precipitation fractionation was employed as an effective method. Firstly, the crucial CMS compound was dissolved in 10 ml of DCM and heated in a water bath to 45 °C. Meanwhile, hexane was slowly added until the solution achieved a steady cloudy point. When the mixture settled down to room temperature, two layers were clearly separated. The second layer, the concentrated polymer gel phase, was collected and assessed to be the CMS copolymers. Pure CMS polymers could be achieved by repeating the same procedure 3 times (Yield: 40 − 55 %).

2.5. Preparation of aqueous dispersions of CMS nanocarriers

All the CMS nanocarriers aqueous dispersions were prepared by an organic solvent-free method. Briefly, 1 ml of MilliQ water was added into each small vial containing 5 mg of CMS 1, CMS 2, and CMS 3. Besides CMS 1, which can be dissolved

directly, the other two were heated to 55 °C for minutes to get clear solutions. Then the solutions were ultrasonicated for 10 min at room temperature.

2.6. Drug encapsulation

A dexamethasone (Dexa) stock solution in acetone at 5 mg/mL concentration was first prepared. Afterwards, 100 μL of the drug stock solution was transferred into small sample vials. The solvent was evaporated completely by placing those vials under high vacuum overnight. 1 mL of the CMS nanocarrier aqueous solution or distilled water as a control was added. The samples were stirred at 1200 rpm for 24 h and filtered by 0.45 μm RC filters to remove the remaining solid Dexa to afford Dexa@CMS.

2.7. Release studies of Dexa@CMS

Drug release study was performed at 37 °C in phosphate buffered saline (PBS, pH 7.4). 0.6 ml of medium containing 9 mg of Dexa @CMS 2 was placed in a dialysis bag (MWCO 3.5 kDa). The dialysis bag was immersed into 15 mL of PBS. The system was kept in an incubator shaker (New Brunswick Scientific Co. Int.) at 37 °C for 24 h. During this time, samples of 5 mL volume were periodically removed and the same volume of fresh PBS was replenished. The amount of released Dexa was determined by HPLC. The release studies were performed in triplicate and the error bars in the plot represent the standard deviation.

2.8. Degradation study of CMS nanocarrier

The degradation of CMS nanocarrier was performed in presence of Novozym 435. Briefly, 5 mg of CMS 2 in PBS solution was prepared, followed by adding 200 wt% of Novozym 435 and 5 μL of n-butanol. After incubating the sample for 24 h at 37 °C, the immobilized enzyme was removed by centrifugation. The supernatant was freeze-dried and the obtained lyophilisate was dissolved in DMSO-d_6. The insoluble salts were removed again by centrifugation and the supernatant was analyzed via ^{1}H NMR.

2.9. Cell viability assays

The cytotoxicity of CMS nanocarriers was estimated by both MTT assay and real time cell analysis (RTCA) method with HaCat cells, keratinocytes from adult human skin. For the MTT assay, the cells were seeded into 96-well plates at a concentration of 10,000 cells per well. After 24 h incubation, the culture medium was removed and replaced with 100 μL of fresh medium containing different concentrations of CMS nanocarriers. The cells were incubated for another 24 h, and then 20 μL of pre-prepared MTT solution was added to each well. After 2 h of incubation, the culture medium as well as the unreacted MTT agent was carefully removed. In each well, 100 μL of DMSO was added to dissolve the blue formazan crystals. The optical density was measured by a microplate reader at 490 nm. Cells treated without CMS carriers were used as a control. For the RTCA assay, 50 μL of cell culture medium was added to each well of the E-plate 96 (Roche, Mannheim, Germany) for the back ground measurement, which was followed by adding HaCat cells at a concentration of 10,000 cells per well. After 24 h incubation, CMS nanocarrier solutions were added. The real-time cell electronic sensor

(RT-CES) system could monitor the cell proliferation and viability in real time. The results were reported as the mean value of triplicates for each sample. The E-plate was incubated with 5% CO_2 at 37°C and monitored on the RTCA SP system (Roche, Mannheim,Germany) with time intervals of at least 15 min for 48 h after treatment. Analysis was performed using the RTCA software version 1.2.1.

2.10. Cellular uptake

HaCat cells and mouse macrophages (J774A.1) were seeded on a 24-well plate at 2.5×10^4 cells per well and cultured for 24 h, and then treated with a cell-culture medium containing FITC-CMS 2 at a final FITC concentration of 2 μg/mL, which was followed by additional 4 h and 24 h incubation, respectively. The cell nuclei were stained with DAPI (Invitrogen, Germany) and the cell membrane was stained with Wheat Germ Agglutinin – Alexa Fluor 594 (Invitrogen, Germany) for 30 min. Afterwards, the cells were rinsed with PBS to remove the excess of dyes. The internalization was observed by CLSM (Leica SP8, Germany) and analyzed by Leica Application SuiteX software.

2.11. Skin penetration

To visualize the topical drug delivery behavior of the CMS nanocarriers, the fluorescent dye Nile red was physically encapsulated into CMS 1−3 and FITC-CMS 2 [22] according to the same procedure as the Dexa encapsulation. A conventional base cream served as a reference. All the formulations contained the same Nile red

concentration (0.0004%, w/w). Human skin (obtained from cosmetic surgeries with informed consent) was thawed and discs of 2 cm diameter were punched and mounted onto static-type Franz cells (diameter 15 mm, volume 12 mL, PermeGear Inc., Bethlehem, PA, USA) with the horny layer facing the air and the dermis having contact with the receptor fluid PBS (pH 7.4, 33.5 °C), stirred at 500 rpm. After 30 min, 35.4 µl of the test formulation was applied onto the skin surface (finite-dose approach) and remained there for 6 h. Subsequently, the skin was removed from the Franz cells, and the skin surface was gently cleaned using PBS. Afterwards, treated skin areas were punched, embedded in a tissue freezing medium (Jung, Nussloch, Germany) and stored in Peel-Aways (Polyscience, Eppelheim, Germany) at −80 °C. For data evaluation, the skin discs were cut into vertical slices of 8 µm thickness using a freeze microtome (Frigocut 2800 N, Leica, Bensheim, Germany). The slices were subjected to normal light and fluorescence light. Nile red amounts in the dermal layers of interest were determined using the fluorescence microscope. Nile red amounts in the dermal layers of interest were determined using the fluorescence microscope (BZ-8000, objectives 20x/0.75, zoom 10x, Plan-Apo, DIC N2, Keyence, Neu-Isenburg, Germany) and slices were subjected to normal light and fluorescence light (red channel: 1/10 s). Relative dye content in skin layers of three skin sections per sample were determined by integration of arbitrary pixel brightness units (ABU) using BZ image analysis software (Keyence, Neu-Isenburg, Germany). Experiments were repeated at three individual donors.

3. Result and discussion

3.1. Synthesis and characterization of hPG-PCL_m-mPEG CMS nanocarriers

Well-defined amphiphilic core-multishell copolymers hPG-PCL_m-mPEG were synthesized via the combination of ring-opening polymerization (ROP) and amide coupling reaction, as illustrated in Scheme 1. Three amphiphilic linear block copolymers mPEG-PCL_m-OH with different lengths of PCL segments were synthesized via ROP of 3-caprolactone (CL) using mPEG (M_n = 2000 g/mol) as a macro-initiator and $Sn(Oct)_2$ as the catalyst. The degree of polymerization (DP) of the PCL segments was calculated by ^{1}H NMR analysis (Fig. S1). By calculating the integral ratio of the peak at 3.35 ppm that originated from the methyl group of mPEG, and the peak at 4.2 ppm that originated from the methylene group (-CH_2-**CH_2**-O-) in the PCL backbone, the DP of the PCL segments were about 5, 10, and 20, respectively, which are in line with the used feed ratios. In the next step, the terminal hydroxy group of mPEG-PCL_m-OH was converted into carboxyl terminal group by reacting with excess amount of succinic anhydride (SA) using DMAP as the catalyst. The ^{1}H NMR spectrum of mPEG-PCL_m-COOH showed a new peak at 2.65 ppm (-COC**H_2**C**H_2**COOH), which confirmed the successful synthesis of the compound. In the final step, amide coupling chemistry was employed to form the hyperbranched core-multishell hPG-PCL-mPEG copolymers from the carboxylic acid-terminated mPEG-PCL double shell and the amino-terminated hPG core. The coupling reaction was carried out in dry DMF at room temperature with HSTU and DIPEA. In order to achieve high functionality, the reaction was performed for 5 days. In the ^{13}C NMR spectra (Fig. S2), the peak at 173.9 ppm assigned to the end

carbonyl group of mPEG-PCL$_m$-COOH (-**C**O-OH) disappeared and a new peak at 172.7 ppm of the carbonyl amide (-**C**ONH-) was observed. FT-IR analysis (Fig. S3) provided additional structural information about the hyperbranched core multi-shell copolymer hPG-PCL$_m$-mPEG. The absorption peak located at 1670 cm^{-1} and 1550 cm^{-1} could be attributed to amide band I and band II, which further proved the successful formation of hPG-PCL$_m$-mPEG CMS copolymers. Fig. S4 shows the GPC diagrams of the CMS 1–3 and their corresponding shells. After coupling, the linear shells have been effectively removed from the CMS particles. The presence of a shoulder peak of CMS suggested that part of the CMS nanoparticles has a lower functionality which might be due to the inhomogeneous distribution of hPG core during synthesizing. The average number of arms per CMS 1−3 molecule was estimated to be about 30, according to the molecular weights determined by GPC, as shown in Table 1.

DSC results from first heating scan of all copolymers are listed in Table 1. The shell 1 - 3 exhibit the melting points 53, 51 and 46 °C, respectively. The higher melting points of the shell 1 and 2 are most likely attributed to the mPEG segments [23]. After coupling the shell to hPG, the melting point of the resulting CMS was clearly decreased to 43 – 48 °C, suggesting the reduced crystallinity of the CMS nanocarriers. Besides, FT-IR was employed to further confirm that the crystallinity of PCL block was reduced after coupling. The bands at 1731 and 1723 cm^{-1} are assigned to the ν(C=O) modes of PCL chains located in the amorphous and crystalline phases, respectively [24]. As shown in Fig. S3d, the absorption of the crystalline phase is much stronger than that of the amorphous one in shell 2. Upon grafting onto hPG, the absorption at 1723 cm^{-1}

becomes weak, and shifts to 1731 cm^{-1}, indicating that the crystallization of PCL blocks has been significantly suppressed in the core-multishell architecture due to the irregular core structure.

3.2. Aggregation properties of hPG-PCL_m-mPEG

Multi- or uni-molecular aggregation behaviors of the CMS nanocarriers were studied by measuring the size in different solvents via DLS, and the results are shown in Table 1. In water, a bigger particle size was observed for both the CMS nanocarriers and the micelles self-assembled from the diblock shells upon increasing the PCL shell length from 5 units to 20 units. The hydrodynamic sizes of CMS nanocarriers were generally larger than the self-assembled micelles, which might be due to the introduced hPG core that has a certain size and its hyperbranched topological structure could also reduce the PCL chain –chain interaction, resulting in a less compact core-shell structure. Additionally, we also studied the size of all the polymers in THF. Since THF is a medium polar solvent which can solubilize both the polar and non-polar parts of these polymers, the size determined in THF was thought to be the size of a single molecule. The CMS nanocarriers could maintain their structures around 15 - 17 nm in THF, but in the case of the linear double shells, only single chains around 1 - 2 nm were observed. This result demonstrated well the covalently interconnected core-multishell structures of the CMS nanocarriers. It is noteworthy that the particle sizes of CMS 1 and CMS 2 in water were quite close to their single molecular sizes determined in THF, which suggests that both copolymers mostly formed unimolecular particles in water.

Meanwhile, the particle size of CMS 3 measured in water (36 nm) was two times larger than in THF (16.8 nm), which suggests that small multi-molecular aggregates are formed. Bigger aggregates though with diameters around 200 nm were observed for all three CMS particles in the intensity distribution of the DLS measurements, as shown in Fig. S5. These aggregates could not be observed in the volume or number distribution and can therefore be considered as a minor pronounced species. The formulation of unimer or multi-molecular aggregates of these core-multishell architectures therefore highly depends on the molecular weight ratio of the hydrophilic and lipophilic segments. Aggregation behaviors of similar star-shape architectures have been reported before. In those publications, similar results (both unimer and multi-molecular aggregates) have also been observed [25]. The Cryo-TEM image clearly shows the morphology of CMS 2 (Fig. 2) and reveals the presence of fairly monodisperse and spherical nanoparticles with diameters of 10 - 15 nm, which is slightly smaller than the size of a CMS unimer determined by DLS due to poor contrast of the PEG shell.

3.3. Encapsulation studies

The anti-inflammatory drug Dexamethasone was selected as a model for the encapsulation studies. The resulting drug loading capacities and efficiencies are given in Table 2. With the increased length of PCL segments, both the drug loading capacity and efficiency improved, which demonstrated that the drug was being solvated by the hydrophobic interations with PCL chains. Interestingly, there was also a significant difference of drug loading capacity between CMS nanocarriers and the respective

amphiphilic linear shells, even though they had the same PCL length. For example, shell 1 had the drug loading capacity 1.3 wt% while CMS 1 had the value of 1.6 wt%. Therefore a 23% higher drug loading capacity was obtained. Also for the CMS 2 and CMS 3, there were 60% and 39% increase respectively in the drug loading capacity, which verified that dendritic core-multi shell carriers are much more efficient than the corresponding block copolymers for guest encapsulation. A possible explanation for the significantly increased drug loading capacity can be due to the lower crystallinity of the CMS nanocarriers. It is also remarkable that all the particle sizes decreased after the CMS nanocarriers were loaded with Dexa. This phenomenon was even more significant in CMS 3, because its particle size after Dexa loading was two times smaller than in the original one, which suggests that the drug can break the aggregates down into unimers. This behavior might be attributed to the collapse of the PCL chains around the Dexa molecules that were embedded inside the hydrophobic pocket, thereby preventing the PCL chains from molecular interaction. A similar phenomenon was observed by Brooks and coworkers [26], when pyrene was encapsulated into amphiphilic hyperbranched copolymers.

3.4. Release and degradation study

The drug release profile of the CMS 2 in PBS is shown in Fig 3a. A relatively fast release rate within 10 h was observed, during which almost 90% of the Dexa was released from the nanocarrier. The efficient release, resulting from the use of the low molecular weight CL oligomers, might maximize the drug bioavailability for skin disease treatment. The biodegradability of CMS 2 in presence of Novozym 435 was

investigated by ^{1}H NMR, shown in Fig. 3b. After 24 h incubation with Novozym 435, a set of new peaks at 2.0 (-C**H**$_2$-COOH), 1.35 (HOOC-CH$_2$-C**H**$_2$-) - 1.45 (-C**H**$_2$-CH$_2$-OH) ppm appeared, which demonstrated the ester bonds in the PCL backbone can be degraded. By calculating the ratio of the integrated area of peak at 2.0 ppm to the sum of the areas of peaks at 2.26 (methylene group neighboring the ester) and 2.0 ppm, a degradation of 35 % can be estimated after 24 h.

3.5. Cytotoxicity

Since nanocarriers might be able to make a connection with viable keratinocytes, we studied the cytotoxicity of the CMS nanocarriers towards HaCat cells, a kind of keratinocytes. MTT (Fig. 4a) results show that all the blank CMS nanocarriers have little toxicity after 24 h, even at a high nanocarrier concentration up to 500 μg/ml. The cytotoxicity was further confirmed by RTCA. As shown in Fig. 4b, the CMS did not induce any obvious reduction in the cell index (CI) values of all the concentrations during the 48 h measurement. Hence, the CMS nanocarriers were not toxic towards HaCat cells in the tested concentration range.

3.6. Cellular uptake

Topical delivery of substances through the continuous stratum corneum can be divided into transcellular and intercellular routes [25]. To test whether the CMS nanocarriers could possibly penetrate transcellularly, we also studied the cellular uptake of CMS nanocarriers towards keratinocytes and macrophages with confocal

microscopy. As shown in Fig. 4c, almost no CMS signals (green) could be detected in the keratinocytes cells after 4 hours incubation. Even with a prolonged incubation time up to 24 h, the CMS signals in the cells were still limited. In contrast, strong CMS signals could be detected in macrophages under the same conditions, which suggests the cellular uptake of CMS nanocarriers towards the keratinocytes was unfavorable, most likely because of the high functional densities of the mPEG arms in the outer shell of the CMS nanocarriers. This also indicates that penetration of the CMS nanocarriers is unfavorable by the transcellular route.

3.7. Skin penetration

For skin penetration studies, Nile red as a model drug was loaded into the CMS nanocarriers or an oil-in-water base cream. All the formulations contained the dye Nile red at the identical concentration of 0.0004%. Fig. 5a shows fluorescence microscopy pictures representing the vertical human skin slices obtained after incubation with the above-mentioned formulations after 6 h. With conventional cream, the weak fluorescence signal is mainly located in the superficial skin layer. On the other hand, with the CMS nanocarriers, the fluorescence faded away from the stratum corneum to the deeper skin layers, which indicated a better dye penetration into the different skin layers with nanocarriers compared to the conventional cream. Also much higher fluorescent intensities were observed in this case. For a more detailed study, corrected arbitrary pixel brightness values of the skin sections were recorded in Fig. 5b. Nile red loading to CMS nanocarriers enhanced the uptake about 3 – 4 fold in both the stratum

corneum and superficial dermis and 4 - 7 fold in the viable epidermis compared to the uptake from the cream. Comparing all the three CMS nanocarriers, the CMS 2 with the medium length of PCL arms (10 repeat units) showed the best penetration enhancement. It is hypothesized that the better penetration enhancement of CMS 2 is related to its proper size and amphiphilicity. In general, the penetration rate is closely related to both diffusion rate and solubility in the penetration matrix [27]. The diffusion rate mainly depends on the size of molecule, and the solubility can be estimated by the hydrophilic and lipophilic balance (HLB). CMS 3 has a significantly larger size (~ 36 nm) compared to the other two nanocarriers (18 - 22 nm) and shows a slower diffusion rate. CMS 1 and CMS 2 have a similar size, but CMS 2 has a lower HLB value, therefore it can interact with skin lipid more effectively and thus results in a better penetration enhancement.

In order to determine how CMS nanocarriers enhance the cargo penetration into skin, we labeled the best candidate CMS 2 covalently with FITC. A skin penetration study of Nile red-loaded FITC-CMS 2 particles was performed. As shown in Fig. 5c, after 6 h treatment, the FITC signals were exclusively captured in the stratum corneum rather than the deeper skin layers, whereas, the Nile red signals diminished from the skin surface into the underlying skin as observed before. This result confirmed that the CMS 2 carriers themselves cannot penetrate the viable skin layer in this time range. However they support the transport of the Nile red through the stratum corneum. The enhanced fluorescence signals in the epidermis and upper dermis are due to the passive diffusion of the released dye.

4. Conclusion

In summary, biodegradable core-multishell nanocarriers were synthesized with combined advantages of an easy scale-up, excellent stability, good cell compatibility, high drug transport capacity, and most importantly, efficient skin penetration enhancement. In aqueous media, the CMS 1 and CMS 2 nanocarriers exist mainly as stable unimolecular systems, whereas CMS 3 with the largest PCL inner shell is prone to form small aggregates. All these CMS nanocarriers are in the size range of 18 – 36 nm. These small-sized nanocarriers facilitate the diffusion in the SC and thus result in highly improved penetration of the released drug. The poor uptake of the nanocarriers in keratinocytes suggests that the skin penetration occurs most likely by an intercellular mechanism (Fig. 6). Even though the average size of the CMS 2 nanocarrier is close to the cut-off level defined by the SCCP (~ 20 nm) [28], penetration of CMS nanocarriers into viable skin layers was not observed for at least 6 hours, which suggest that they are safe as skin penetration enhancers. We expect that these nanocarriers designed and based on the dendritic core-multishell topology can provide new avenues for efficient topical drug delivery and skin therapy.

Acknowledgements:

We would like to thank SFB 1112, Chinese Scholar Council (CSC) and the Focus Area Nanoscale of Freie Universität Berlin for the financial support and thank PD Dr. Christoph Böttcher and the Core-Facility BioSupraMol for Cryo-TEM measurements.

We would like to thank Dr. Pamela Winchester for proofreading this manuscript.

References

[1] M. Brazil, Principles of penetration, Nat. Rev. Drug. Discov. 4 (2005) 372−373.
[2] M.R. Prausnitz, S. Mitragotri, R. Langer, Current status and future potential of transdermal drug delivery, Nat. Rev. Drug. Discov. 3 (2004) 115−124.
[3] J.D. Bos, M.M.H.M. Meinardi, The 500 Dalton rule for the skin penetration of chemical compounds and drugs, Exp. Dermatol. 9 (2000) 165−169.
[4] M.M. Badran, J. Kuntsche, A. Fahr, Skin penetration enhancement by a microneedle device (Dermaroller®) in vitro: Dependency on needle size and applied formulation, Eur. J. Pharm. Sci. 36 (2009) 511−523.
[5] E.H. Choi, S.H. Lee, S.K. Ahn, S.M. Hwang, The pretreatment effect of chemical skin penetration enhancers in transdermal drug delivery using iontophoresis, Skin Pharmacol. Physiol. 12 (1999) 326−335.
[6] A. Maruani, E. Vierron, L. Machet, B. Giraudeau, A. Boucaud, Efficiency of low-frequency ultrasound sonophoresis in skin penetration of histamine: A randomized study in humans, Int. J. Pharm. 385 (2010) 37−41.
[7] A. Coutel-Egros, Y. Maitani, M. Veillard, Y. Machida, T. Nagai, Combined effects of pH, cosolvent and penetration enhancers on the in vitro buccal absorption of propranolol through excised hamster cheek pouch, Int. J. Pharm. 84 (1992) 117−128.
[8] D.D. Verma, S. Verma, G. Blume, A. Fahr, Liposomes increase skin penetration of entrapped and non-entrapped hydrophilic substances into human skin: a skin penetration and confocal laser scanning microscopy study, Eur. J. Pharm. Biopharm. 55 (2003) 271−277.
[9] S.A. Wissing, R.H. Müller, Solid lipid nanoparticles as carrier for sunscreens: in vitro release and in vivo skin penetration, J. Control. Release 81 (2002) 225−233.
[10] C. Valenta, B.G. Auner, The use of polymers for dermal and transdermal delivery, Eur. J. Pharm. Biopharm. 58 (2004) 279−289.
[11] F. Du, H. Meng, K. Xu, Y. Xu, P. Luo, Y. Luo, W. Lu, J. Huang, S. Liu, J. Yu, CPT loaded nanoparticles based on beta-cyclodextrin-grafted poly(ethylene glycol)/poly (l-glutamic acid) diblock copolymer and their inclusion complexes with CPT, Colloid Surf. B 113 (2014) 230−236.
[12] D. van der Merwe, J.D. Brooks, R. Gehring, R.E. Baynes, N.A. Monteiro-Riviere, J.E. Riviere, A physiologically based pharmacokinetic model of organophosphate dermal absorption, Toxicol. Sci. 89 (2006) 188−204.
[13] R. Alvarez-Román, A. Naik, Y.N. Kalia, R.H. Guy, H. Fessi, Skin penetration and distribution of polymeric nanoparticles, J. Control. Release 99 (2004) 53−62.
[14] J. Shim, H. Seok Kang, W.-S. Park, S.-H. Han, J. Kim, I.-S. Chang, Transdermal delivery of mixnoxidil with block copolymer nanoparticles, J. Control. Release 97 (2004) 477−484.
[15] M. Lapteva, K. Mondon, M. Möller, R. Gurny, Y.N. Kalia, Polymeric micelle nanocarriers for the cutaneous delivery of tacrolimus: A targeted approach for the treatment of psoriasis, Mol. Pharm. 11 (2014) 2989−3001.
[16] M.R. Radowski, A. Shukla, H. von Berlepsch, C. Böttcher, G. Pickaert, H. Rehage, R. Haag,

Supramolecular aggregates of dendritic multishell architectures as universal nanocarriers, Angew. Chem. Int. Ed. 119 (2007) 1287−1292.
[17] E. Fleige, B. Ziem, M. Grabolle, R. Haag, U. Resch-Genger, Aggregation Phenomena of Host and Guest upon the loading of dendritic core-multishell nanoparticles with Solvatochromic dyes, Macromolecules 45 (2012) 9452−9459.
[18] S. Xu, Y. Luo, R. Graeser, A. Warnecke, F. Kratz, P. Hauff, K. Licha, R. Haag, Development of pH-responsive core–shell nanocarriers for delivery of therapeutic and diagnostic agents, Bioorgan. Med. Chem. Lett. 19 (2009) 1030−1034.
[19] S. Küchler, M.R. Radowski, T. Blaschke, M. Dathe, J. Plendl, R. Haag, M. Schäfer-Korting, K.D. Kramer, Nanoparticles for skin penetration enhancement – A comparison of a dendritic core-multishell-nanotransporter and solid lipid nanoparticles, Eur. J. Pharm. Biopharm. 71 (2009) 243−250.
[20] E. Fleige, K. Achazi, K. Schaletzki, T. Triemer, R. Haag, pH-Responsive dendritic core–multishell nanocarriers, J. Control. Release 185 (2014) 99−108.
[21] S. Roller, H. Zhou, R. Haag, High-loading polyglycerol supported reagents for Mitsunobu- and acylation-reactions and other useful polyglycerol derivatives, Mol. Divers, 9 (2005) 305−316.
[22] Z. Xu, S. Zhu, M. Wang, Y. Li, P. Shi, X. Huang, Delivery of paclitaxel using PEGylated graphene oxide as a nanocarrier, ACS Appl. Mater. Interfaces 7 (2015) 1355−1363.
[23] M.G. Carstens, J.J.L. Bevernage, C.F. van Nostrum, M.J. van Steenbergen, F.M. Flesch, R. Verrijk, L.G.J. de Leede, D.J.A. Crommelin, W.E. Hennink, Small oligomeric micelles based on end group modified mPEG−oligocaprolactone with monodisperse hydrophobic blocks, Macromolecules 40 (2007) 116−122.
[24] Y. He, Y. Inoue, Novel FTIR method for determining the crystallinity of poly(ε-caprolactone), Polym. Int. 49 (2000) 623−626.
[25] C. Rabe, E. Fleige, K. Vogtt, N. Szekely, P. Lindner, W. Burchard, R. Haag, M. Ballauff, The multi-domain nanoparticle structure of a universal core-multi-shell nanocarrier, Polymer 55 (2014) 6735−6742.
[26] R.K. Kainthan, C. Mugabe, H.M. Burt, D.E. Brooks, Unimolecular micelles based on hydrophobically derivatized hyperbranched polyglycerols: ligand binding properties, Biomacromolecules 9 (2008) 886−895.
[27] H.K. Cho, S. Lone, D.D. Kim, J.H. Choi, S.W. Choi, J.H. Cho, J.H. Kim, I.W. Cheong, Synthesis and characterization of fluorescein isothiocyanate (FITC)-labeled PEO–PCL–PEO triblock copolymers for topical delivery, Polymer 50 (2009) 2357−2364.
[28] SCCP. The Scientific Committee on Cosmetic Products (SCCP) Opinion on Safety of Nanomaterials in Vosmetic Products. http://ec.europa.eu/health/ph_risk/committees/04_sccp/docs/sccp_o_123.pdf (2007)

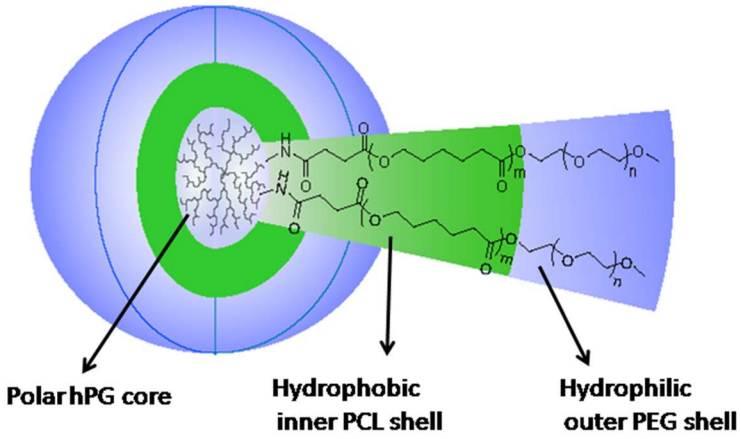

Fig. 1. Structure of core multi-shell (CMS) nanocarriers based on a hyperbranched polyglycerol (hPG) – poly(ε-caprolactone) (PCL) – poly(ethylenglycol)methyl ether (mPEG) architecture.

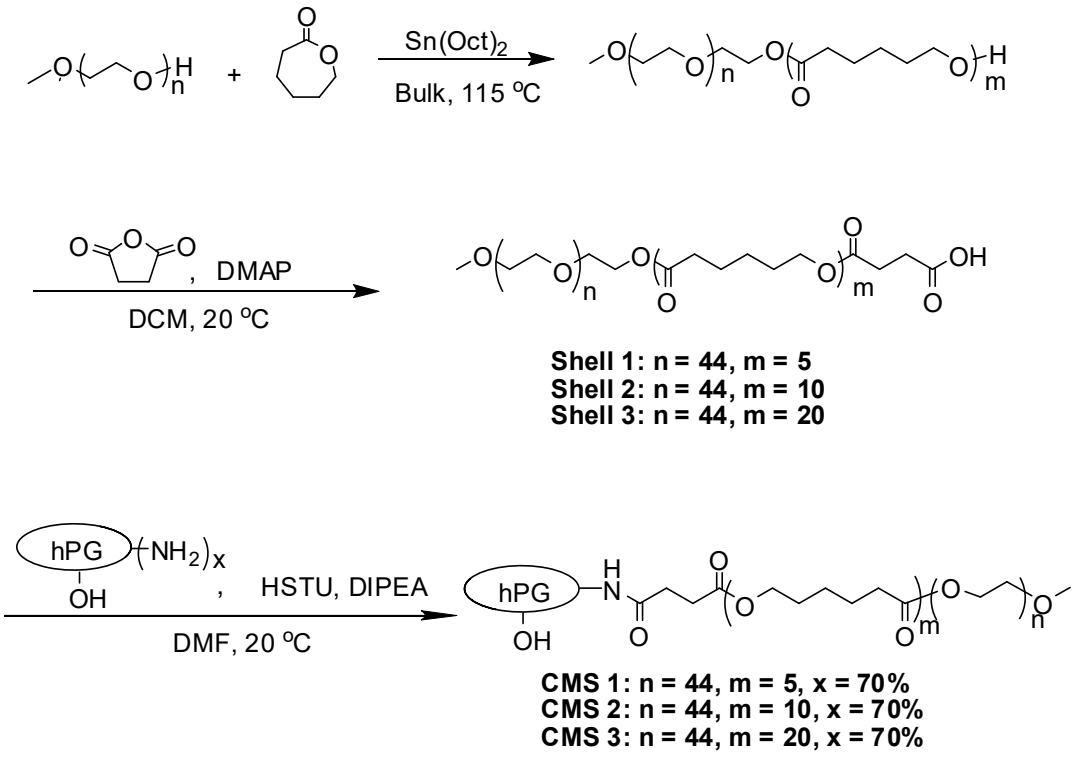

Scheme 1. Synthesis of hPG-PCL$_m$-mPEG core multi-shell architectures (CMS).

Table 1
Characterization of polymers.

Polymer	CL/ PEG ratio[a]	M_n (g/mol) ($\times 10^3$)[b]	PDI (M_w/M_n)	Arm density[c]	T_m (°C)	Size[d]	
						D_h (nm) H_2O	D_h (nm) THF
hPG-NH_2	-	9.8	1.73	-	-	5.5±1.2	-
Shell 1	5	3.4	1.11	-	53.2	11.8±0.7	1.6±0.4
Shell 2	10	4.4	1.14	-	51.7	13.7±1.1	1.4±0.7
Shell 3	20	5.5	1.12	-	46.4	17.9±1.1	2.5±1.3
CMS 1	5	113.7	1.55	31	47.6	18.4±1.3	16.7±1.4
CMS 2	10	139.3	1.42	30	48.3	21.9±0.2	15.2±0.5
CMS 3	20	185.5	1.82	32	43.1	36±6.3	16.8±2.6

[a] The CL/PEG ratios were calculated from ^{1}H NMR integrals.
[b] Molecular weight and polydispersity index of hPG-NH_2were measured by GPC in water, and the others were measured in DMF.
[c] The arm densities were calculate based on the equation $(M_{n\,(CMS)}- M_{n(hPG)})/M_{n(Shell)}$.
[d] The hydrodynamic diameter (D_h) is given based on the volume distribution measured by DLS at concentration 5 mg/mL in Milli Q water. The values represent the maximum of the distribution and the mean standard deviation.

Table 2
Characterization of Dexamethasone loaded CMS nanocarriers.

polymer	LC (wt%)[a]	LC ($mol_{drug}/mol_{carrier}$)	EE (%)	D_h [b](nm)
Shell 1	1.3	0.1	13.4	12.2±0.9
Shell 2	1.5	0.2	14.8	80.1±5.7
Shell 3	2.3	0.3	23.0	-125.6±49.1
CMS 1	1.6	4.6	15.8	19.0±1.0
CMS 2	2.4	10	23.6	17.2±0.3
CMS 3	3.2	15.2	32.2	19.9±0.2

[a] The drug loading capacity was calculated based on equation LC wt% = $W_{\text{loaded drug}}$ / $W_{\text{polymer}} \times 100$, note: Free Dexa amount in water has been deducted during calculation, which is 51 μg/ml by measuring a blank sample via HPLC.
[b] The hydrodynamic diameter (D_h) is given based on the volume distribution measured by DLS at concentration 5 mg/mL in Milli Q water. The values represent the maximum of the distribution and the mean standard deviation.

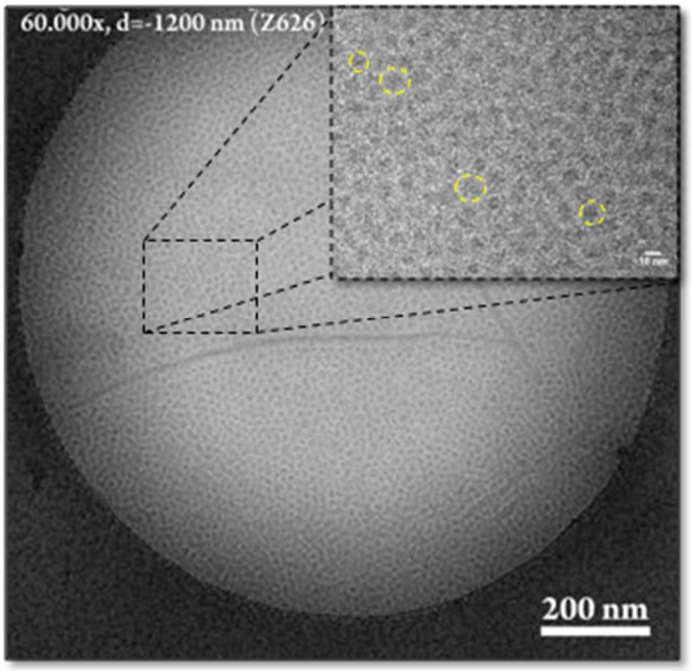

Fig. 2. Cryo-TEM image of CMS 2 nanocarrier at 5 mg/ml. The scale bar for the enlarged view is 10 nm. The inset shows magnification and defocus.

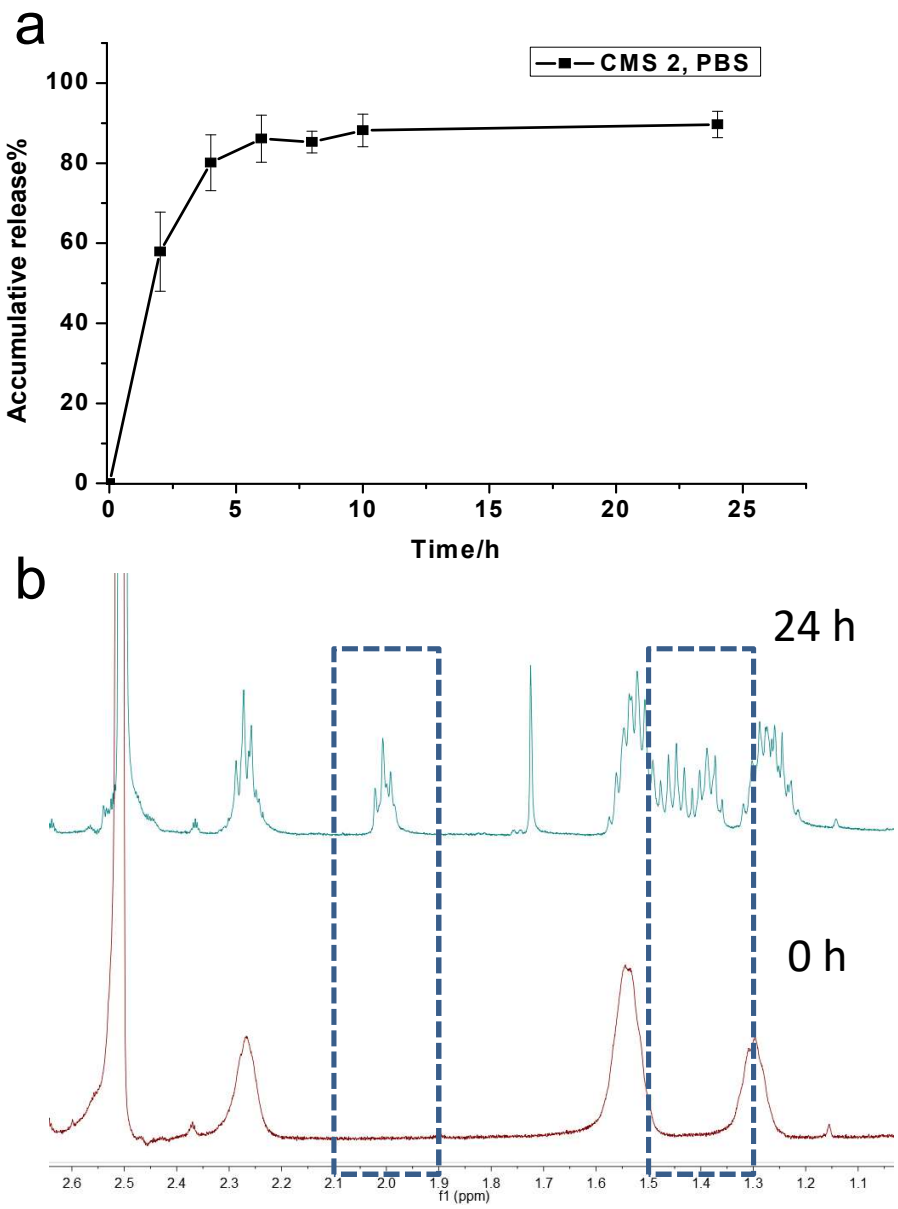

Fig. 3. a) Dexamethasone release profile from CMS 2 at pH 7.4, 37 °C by dialysis method (n = 3); b) ^{1}H NMR spectra (DMSO-d_6, 298 K) of CMS nanocarriers before and after incubation with Novozym 435 for 24 h.

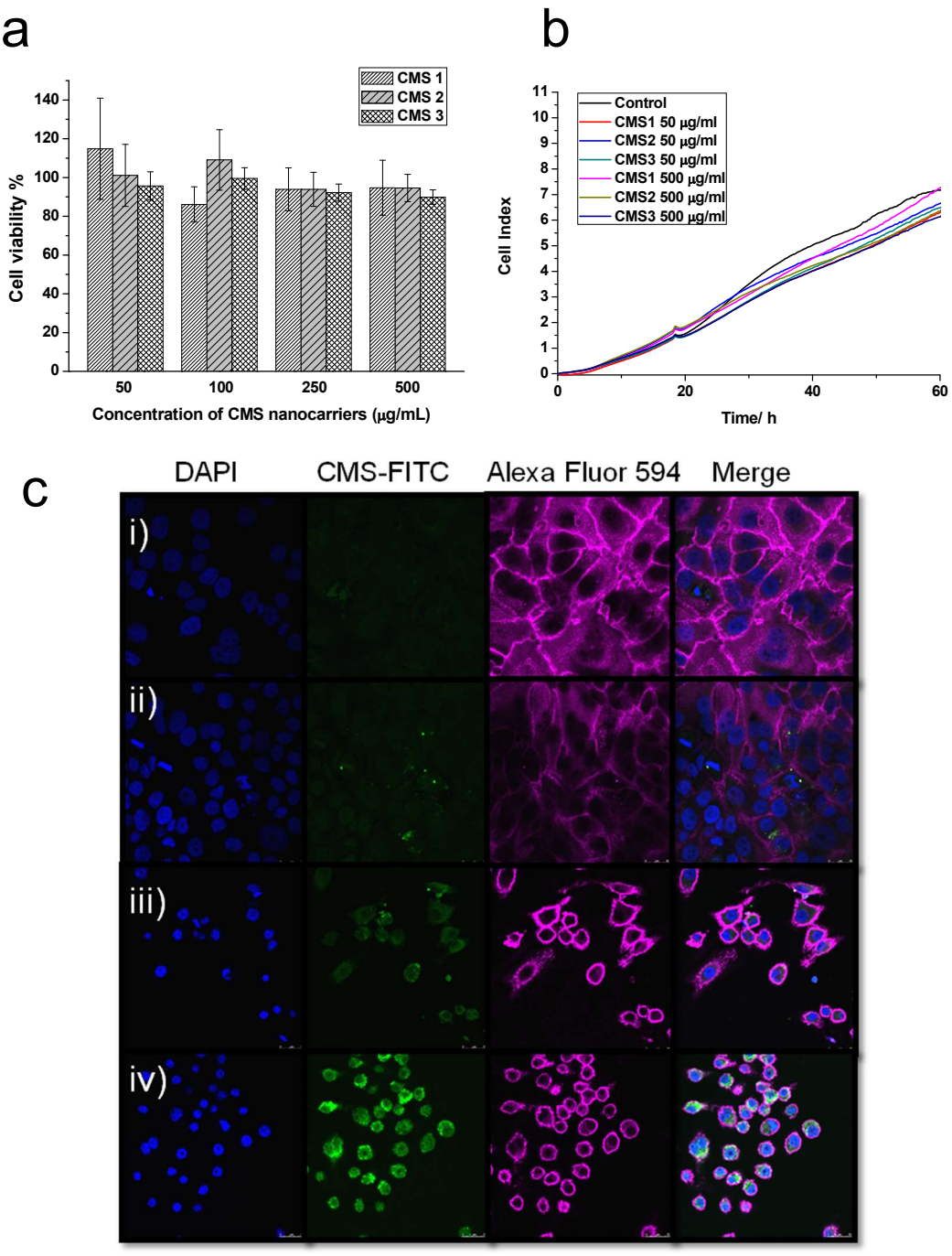

Fig. 4. Cell viability of HaCat cells determined by a) MTT assay for 24 h (n =3). The cell viability of untreated control was set to be 100%; b) RTCA assay; c) Cellular uptake study of CMS 2 towards HaCat cells (keratinocytes) after 4h (i), 24h (ii) and towards macrophages after 4h (iii), 24h (iv).

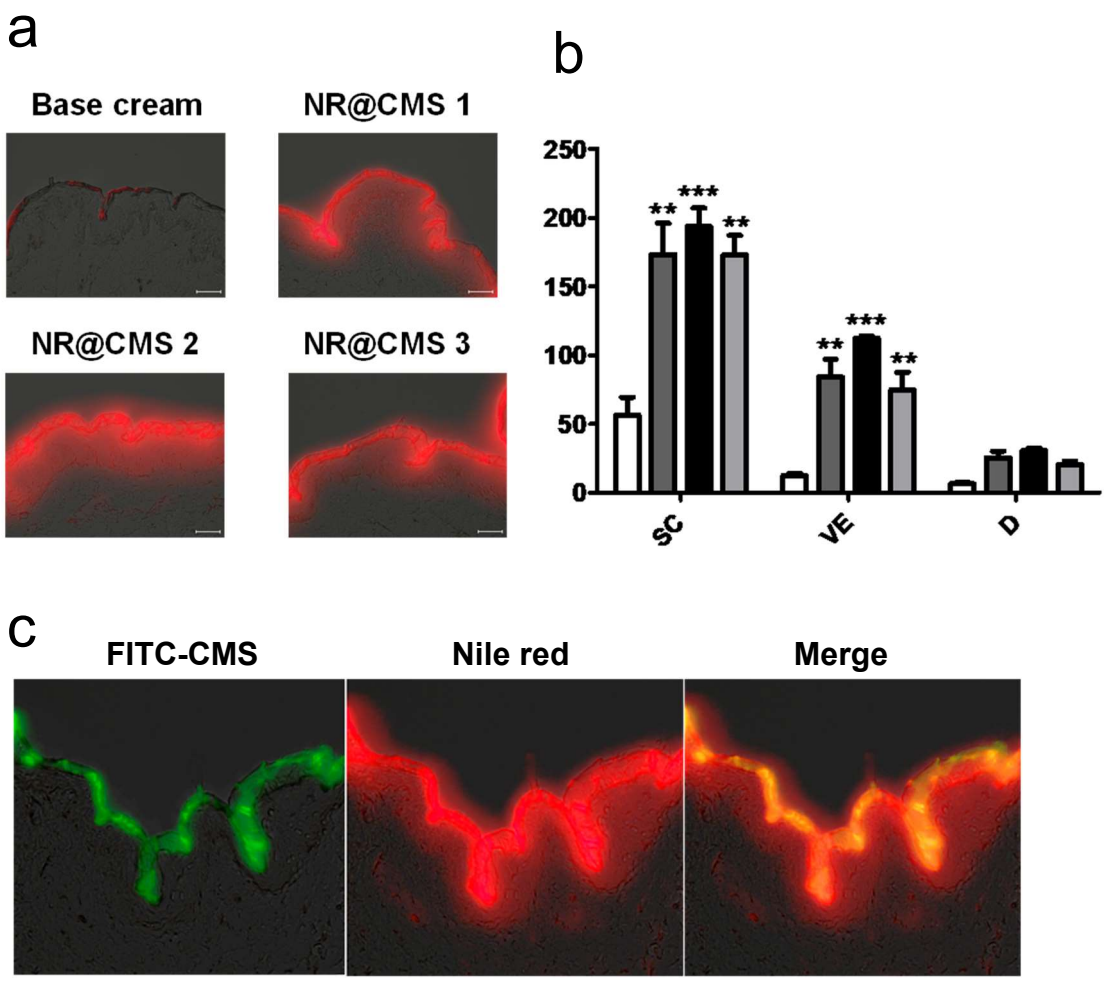

Fig. 5. a) Visualization of skin penetration behaviors of Nile red loaded CMS nanocarriers (NR@CMS1-3), compared to commercial cream in human skin; b) Quantified Nile red amounts in different skin layers (SC: stratum corneum; VE: viable epidermis; D: dermis, n = 3); c) Skin penetration of NR@FITC-CMS 2, observed in FITC and Nile red channel, respectively

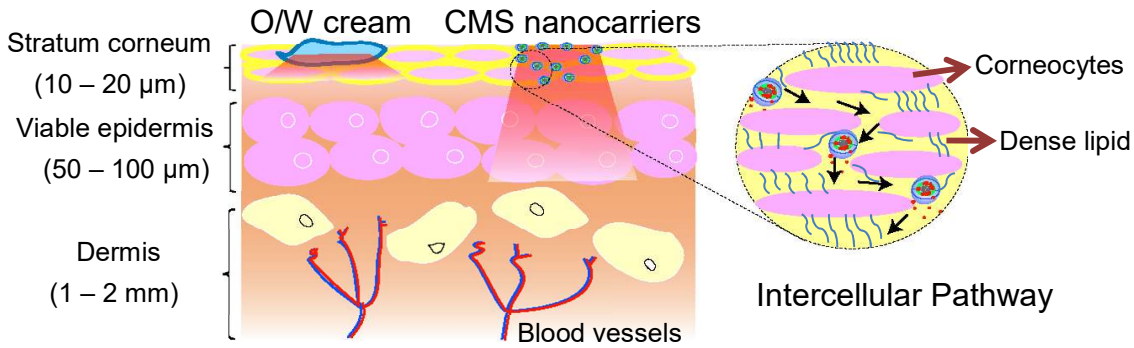

Fig. 7. The suggested penetration enhancement mechanism: Large amount of cargo was transported by CMS into skin by interacting with skin lipids. The released cargo penetrated into deep skin layers and CMS itself stays at superficial stratum corneum layer of skin.